Journal of Power Sources 189 (2009) 1060–1065

Contents lists available at ScienceDirect

Journal of Power Sources

journal homepage: www.elsevier.com/locate/jpowsour

The effect of water content on the electrochemical impedance response and microstructure of Ni-CGO anodes for solid oxide fuel cells

P. Kim [a], D.J.L. Brett [b], N.P. Brandon [c,*]

[a] Department of Chemical Engineering, Mahidol University, Puttamonthon, Nakorn Pathom 73170, Thailand
[b] Department of Chemical Engineering, University College London, WC1E 7JE, United Kingdom
[c] Department of Earth Science and Engineering, Imperial College London, London SW7 2AZ, United Kingdom

ARTICLE INFO

Article history:
Received 6 August 2008
Received in revised form
29 December 2008
Accepted 30 December 2008
Available online 17 January 2009

Keywords:
Solid oxide fuel cell
Anode
Steam
Hydrogen oxidation

ABSTRACT

Using electrochemical impedance spectroscopy, the high frequency (HF) and low frequency (LF) impedance of nickel–gadolinium-doped ceria (Ni-CGO) symmetrical cells (Ni-CGO/YSZ/Ni-CGO) in dry and moist atmospheres were studied. The HF component of the impedance response in moist H_2 varied with operating temperature, while the LF component varied with the H_2 content in the fuel. The EIS response in dry fuel behaved differently. The LF impedance in dry fuel (97% H_2, 3% N_2) showed a large increase, and varied significantly with both temperature and H_2 content in the fuel, while the HF component varied with temperature in a similar manner to that observed in moist fuel. This suggests that the HF impedance in both moist and dry fuel is associated with the charge transfer resistance. The LF impedance in the case of moist fuel can be reasonably attributed to mass transport effects, while that in the case of dry fuel cannot be attributed to the same mass transport process. The estimated time constant of the LF component was considerably larger in dry atmospheres, compared to that in moist conditions. Scanning electron microscopy (SEM) images showed crack formation in the anode cermets exposed to dry atmospheres, which were not evident in cermets exposed to moist conditions.

1. Introduction

Solid oxide fuel cells (SOFCs) are a promising technology for future energy conversion systems due to their high efficiency, ability to generate high grade heat, and fuel flexibility. The efficiency of the fuel cell is known to rely significantly on fuel gas composition. It is known that the electrochemical oxidation of H_2 is strongly influenced by the steam content in the fuel. It has been reported that a small amount of water (few %) significantly helps decrease anode polarization resistance [1–4], while too large an amount of water can degrade anode performance [1,5], especially at high electrical load and low concentrations of H_2 in the fuel. A range of reaction pathways has been proposed to account for fuel oxidation, involving various elementary steps [6–11]. The mechanism by which the steam content in fuels promotes the H_2 oxidation reaction is still not well established. There is contradictory evidence as to whether adsorption of oxygen species from water on the ceramic part of a cermet anode [12,13] or the metal part of the anode [1,14] plays the key role in promoting the reaction.

Exclusive to this study is the consideration of nickel–ceria-based cermet anodes (ceria gadolinium oxide—CGO) designed for use in the temperature range 773–923 K [15], at the lower end of intermediate temperature solid oxide fuel cell (IT-SOFC) operation [16]. The effect of exposure to dry and moist fuel on the electrochemical performance (studied using electrochemical impedance spectroscopy—EIS) and on microstructure (assessed using scanning electron microscopy—SEM) of the cermets is considered in 'dry' H_2 (97% H_2, 3% N_2) and 'moist' H_2 (97% H_2, 3% H_2O) at 873 K.

2. Experimental

2.1. Cermet symmetrical cell fabrication

Symmetrical cells with electrodes composed of nickel–gadolinium-doped ceria (Ni-CGO), deposited on both sides of yttria-stabilised zirconia (YSZ), were fabricated. The Ni-CGO/YSZ/Ni-CGO symmetrical cell configuration, with YSZ as the electrolyte material, was chosen in place of CGO in order to avoid artefacts appearing in the electrochemical impedance response arising from the mixed ionic / electronic conductivity (MIEC) exhibited by CGO in low pO_2 environments at elevated temperatures [17]. YSZ powder (8 mole% Y_2O_3, Tosoh, Japan) was uniaxially pressed (1 tonne, 30 s), followed by sintering at 1723 K in air for 5 h—giving a dense pellet (~95% calculated density) with a diameter of ~11.9 mm and thickness of ~1.27 mm. The NiO-CGO layers, giving the ratio of Ni to CGO after reduction of 50 wt.% $Ce_{0.9}Gd_{0.1}O_{1.95}$ and 50 equiv. wt.%

* Corresponding author. Tel.: +44 2075945704; fax: +44 2075947444.
E-mail address: n.brandon@imperial.ac.uk (N.P. Brandon).

0378-7753/$ – see front matter © 2009 Elsevier B.V. All rights reserved.
doi:10.1016/j.jpowsour.2008.12.150

Ni (NextTech Materials, USA), were deposited on both sides of the dense electrolyte and fired at 1573 K for 2 h. The reduction of NiO to Ni was performed in 97% H_2/3% H_2O for 1 h at the experimental temperature. This resulted in a cermet layer with a thickness of ~100 μm.

2.2. Electrochemical performance measurements using EIS

Electrochemical impedance spectroscopy was performed at open circuit conditions on symmetrical cells. This approach was adopted since EIS allows measurements to be made under pseudo-steady state conditions at open circuit; operation away from open circuit will not give an accurate impression of the effect of fuel steam content due to the local generation of H_2O at the anode surface. EIS was performed using an Autolab PGSTAT30 fitted with a frequency response analyser (FRA) (Autolab, EcoChemie, Netherlands). The instrumentation was controlled using FRA for Windows (version 4.9.004) which allowed fitting of the complex plane impedance data to equivalent circuit models. The non-linear least squares fit was performed using the approach of Boukamp [18]. Impedance measurements were performed in potentiostatic mode using a sinusoidal signal amplitude of 20 mV_{rms}, over the frequency range of 10 kHz to 10 mHz. Fig. 1(a) shows the head of the test rig used for the impedance measurement. Electrical connection was made to the electrodes of the symmetrical cells via platinum wires connected to a fine platinum mesh (mesh 99.99% Pt, 0.06 mm wire diameter, 0.25 mm aperture; wire 99.99% Pt, 0.25 mm diameter, both GoodFellow, UK) and put into compression using the two tie rods (Inconel) shown, with springs in tension outside of the furnace hot zone. The cell holder was then placed inside a quartz tube, with gas inlet and outlet points, so allowing the gaseous environment exposed to the cell to be controlled. A tube furnace (Lenton, UK) was used to control the temperature of the rig.

Fig. 1(b) shows the experimental set-up for the delivery of gas to the samples in the furnace. The test system allows different compositions of H_2S, H_2, N_2, and H_2O to be introduced to the cell. The H_2 and N_2 gas lines (both 99.99%, BOC, UK) connect to calibrated mass flow controllers (Bronkhorst, UK) which are available for gas flow rates ranging from 20 to 1000 cm^{-3} min^{-1}. After passing through the mass flow controllers, the H_2/N_2 line passes through the humidifier, which is a bubble column situated inside a thermocirculator bath, to humidify the flowing gas with water at the required level. The H_2/N_2 line, which does not pass through the humidifier, is available in parallel for delivering dry fuel.

The electrochemical impedance response was fitted to an equivalent circuit composed of a resistor in series with two parallel constant phase element (CPE)/resistor combinations, shown in Fig. 1(c). The CPE is used, as opposed to a pure capacitance, due to the finite thickness of the porous electrode having a distributed electrochemical response that results in the centre of circular arc being suppressed below the horizontal axis on the complex plane diagram [19,20].

2.3. Microstructure analysis using SEM

SEM images were taken using a LEO 1525 FEGSEM (Zeiss) with an accelerating potential of 5 kV under the vacuum of 1.5×10^{-5} torr. The sample is collected using a N_2-quenching method whereby the gas feed is replaced with dry N_2 and the sample is pulled out of the hot zone (using a K-type thermocouple attached to a ceramic boat holding the sample) of the furnace in to a cool zone as shown in Fig. 1(b). The chemical analysis was done using energy dispersive X-ray (EDX, Oxford Instrument Microanalysis System) with an accelerating potential of 20 kV.

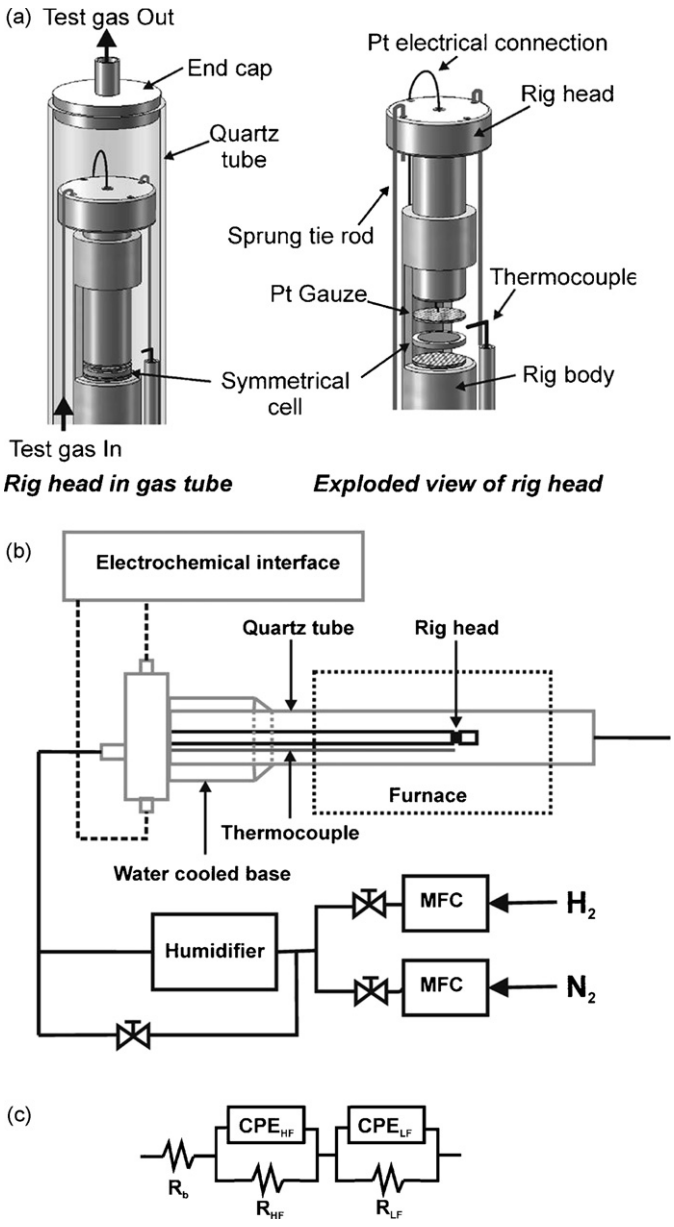

Fig. 1. Test system: (a) head of test rig for electrochemical impedance measurement; (b) test system; and, (c) an equivalent circuit for impedance response fitting.

3. Results and discussion

3.1. Ni-CGO symmetrical cell performance in moist hydrogen

EIS measurements were initially performed on Ni-CGO cermet symmetrical cells (Ni-CGO/YSZ/Ni-CGO) in a humidified atmosphere to establish the base response expected from the cell. Fig. 2 shows that the generic form of the impedance response was composed of two partially resolved arcs, as mentioned. To help determine the origin of these features, the gas composition and temperature were varied to determine how these factors influenced the response. Fig. 2(a) shows how the EIS response varied for H_2 concentrations ranging from 9.7% to 97% (constant 3% H_2O, N_2 balance) at a constant temperature of 873 K, and Fig. 2(b) shows the response when the temperature was varied from 833 K to 873 K at constant H_2 content (97% H_2, 3% H_2O). At constant temperature, the low frequency arc (LF arc) varied significantly with H_2 content (decreasing with increasing pH_2), while the high frequency

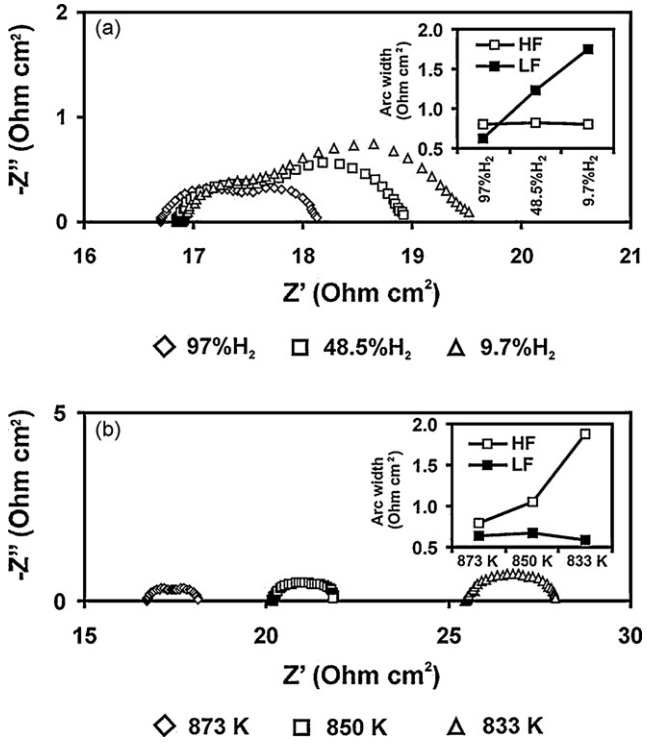

Fig. 2. Electrochemical impedance measurements on symmetrical cells (Ni-CGO/YSZ/Ni-CGO) exposed to humidified atmospheres under varying operating conditions; (a) varied H_2 content from 97% to 9.7% at a constant temperature of 873 K (3% H_2O), the figure inset shows the HF and LF arc width, plotted with H_2 content; (b) impedance response at varied temperature from 838 K to 873 K at a constant H_2 content (97% H_2, 3% H_2O), the figure inset shows the HF and LF arc width plotted with temperature.

arc (HF arc) remained unaffected, as can be seen inset in Fig. 2(a). This contrasts with the response when the temperature was varied while maintaining a constant H_2 concentration of 97%, as shown in Fig. 2(b) and inset. At constant pH_2, the HF arc increased significantly with decreasing temperature, while the LF arc remained effectively constant. This suggests that the HF arc arises from the charge transfer resistance, while the LF arc can be reasonably attributed to mass transport effects. The shift in the position of the arc along the real (Z') axis, associated with operation at different temperatures, is due to a change in the purely ohmic response of the cell which is a consequence of the change in ionic conductivity of the YSZ pellet with temperature, and to a much lesser extent on the ionic conductivity of the CGO in the electrode cermet.

Fig. 3 shows how the impedance response develops with time when a Ni-CGO symmetrical cell is exposed to the gas mixture

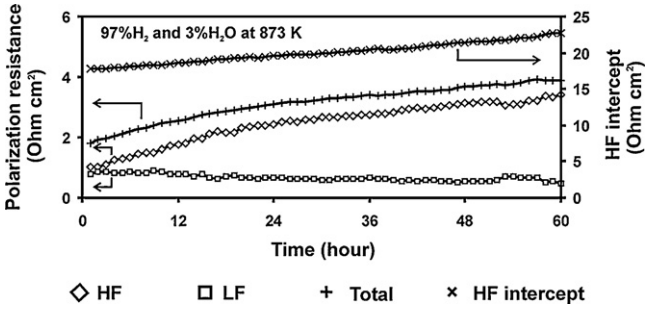

Fig. 3. The plot of impedance response of the Ni-CGO half cell (Ni-CGO/YSZ/Ni-CGO) exposed to 97% H_2 and 3% H_2O at 873 K for 60 h. The plot shows the HF real axis intercept, HF feature, LF feature, and total arc width of the impedance spectra in H_2S-free atmosphere.

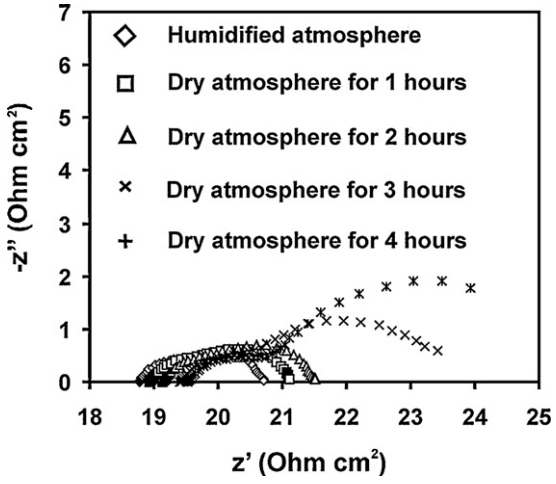

Fig. 4. Electrochemical impedance measurements on symmetrical cells (Ni-CGO/YSZ/Ni-CGO) exposed to humidified atmosphere (97% H_2, 3% N_2, 873 K) and then to dry atmosphere (97% H_2, 3% N_2, 873 K).

of 97% H_2 and 3% H_2O at 873 K for 60 h. The impedance spectra were fitted to the equivalent circuit using a non-linear least squares method, as mentioned previously. The fitted values were plotted separately as the HF, LF, and total arc width, as well as the high frequency intercept of the impedance arc with the real-axis (HF intercept). The total impedance plot shows that the cell performance degraded monotonically with time. Also, it can be seen that an increase in the total arc impedance was entirely due to an increase in the HF feature, while the LF feature remained comparatively stable. Although the total impedance arc width showed a non-linear trend, a linear approximation over the entire 60 h period gave a base degradation rate of 0.03 $\Omega\,cm^2\,h^{-1}$, with the HF intercept exhibiting a linear resistance increase at a rate of 0.08 $\Omega\,cm^2\,h^{-1}$.

When the operating condition was changed from the humidified atmosphere (97% H_2, 3% H_2O, 873 K) to dry atmosphere (97% H_2, 3% N_2, 873 K), the EIS response showed a different impedance shape. The LF impedance gradually increased within 4 h of dry fuel exposure, as can be seen in Fig. 4. The impedance response of the cell under dry condition was then studied and is shown in the following section.

3.2. Ni-CGO symmetrical cell performance in dry hydrogen

Fig. 5 shows the EIS response in dry H_2 when gas composition and temperature were varied. Fig. 5(a) shows the response when the H_2 content was varied from 9.7 to 97% H_2 (balance N_2) at a constant temperature of 873 K. The LF feature increased substantially when the H_2 content decreased, while the HF component remained relatively stable. Fig. 5(b) shows the response when temperature was varied from 838 K to 873 K, while the gas composition was maintained constant at 97% H_2/3% N_2. The EIS response in Fig. 5(b) shows that the HF feature increased with decreasing temperature. This is similar to the case for moist fuel; the HF feature in dry hydrogen is therefore attributed to charge transfer resistance. Compared to the HF feature, the LF feature varied with much larger magnitude (increasing with decreased temperature). The LF feature in the dry fuel case is more complex than that for moist operation since it was observed to vary significantly with both H_2 content and temperature. Moreover, the frequency domain of the LF feature is different in dry fuel and moist fuel. The frequency range of the LF feature in moist fuel is between 0.63 and 0.01 Hz, while the complete LF feature in dry fuel could not be realised due to the limitation of the instrument which has a lower frequency limit

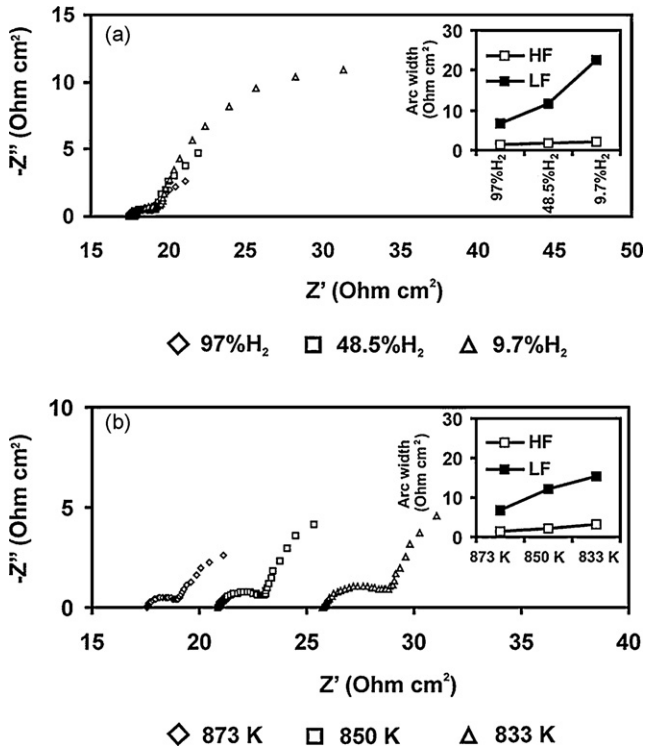

Fig. 5. Electrochemical impedance measurements on symmetrical cells (Ni-CGO/YSZ/Ni-CGO) exposed to dry atmospheres in varying operating conditions; (a) varied H_2 content from 97% to 9.7% (balance N_2) at a constant temperature of 873 K, the figure inset shows the HF and LF arc width, plotted with H_2 content; (b) impedance response at varied temperature from 838 K to 873 K at a constant H_2 content (97% H_2, 3% N_2), the figure inset shows the HF and LF arc width plotted with temperature.

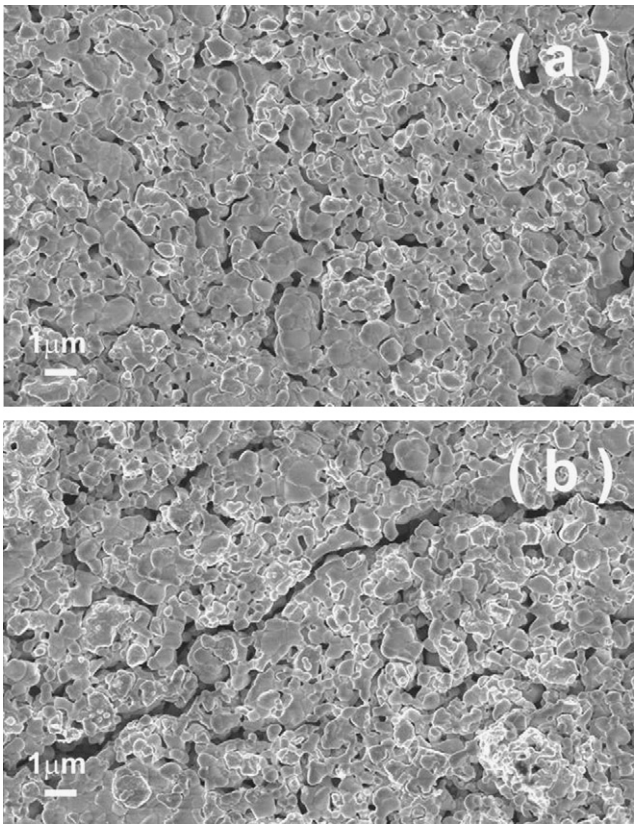

Fig. 7. SEM images of Ni-CGO cermets exposed to (a) moist atmosphere (97% H_2, 3% H_2O, 873 K, 24 h); (b) dry atmosphere (97% H_2, 3% N_2, 873 K, 24 h).

of 0.01 Hz. This suggests that the LF feature in dry fuel cannot be exclusively described as a mass transport effect analogous to that in moist hydrogen conditions.

The cell was exposed to dry fuel (97% H_2, 3% N_2) at 873 K for 60 h. The HF-intercept, HF and LF arc width are shown in Fig. 6. The total degradation rate of the cell in dry fuel is relatively much higher (0.29 $\Omega\,cm^2\,h^{-1}$), compared to that in moist fuel (0.03 $\Omega\,cm^2\,h^{-1}$). Considering the HF and LF impedance, it can be seen that the LF feature significantly increases over time when compared to the HF feature. When the degradation rate of the HF impedance is considered, the rate of HF impedance degradation over time is 0.07 $\Omega\,cm^2\,h^{-1}$. This rate is larger than the degradation rate of the HF impedance in moist fuel. This suggests that using dry fuel has a negative effect on the anode performance, accelerating the increase in both HF and LF impedance.

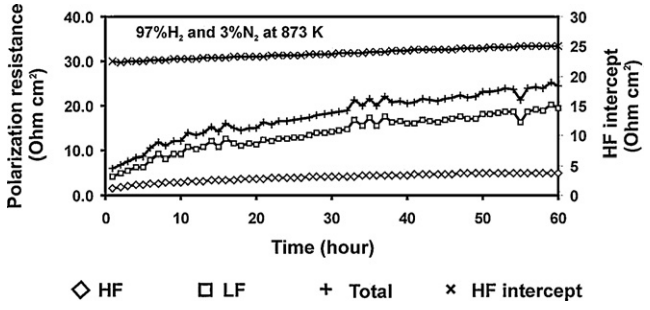

Fig. 6. The plot of impedance response of the Ni-CGO anode half cell (Ni-CGO/YSZ/Ni-CGO) exposed to dry fuel (97% H_2, 3% N_2) at 873 K for 60 h. The plot shows HF real-axis intercept, HF, LF, and total arc width of the impedance spectra in H_2S-free atmosphere.

Fig. 7(a) and (b) show SEM micrographs of a Ni-CGO cermet after exposure to moist H_2 (97% H_2, 3% H_2O, 873 K, 24 h), and after exposure to dry H_2 (97% H_2, 3% N_2, 873 K, 24 h). A clear microstructural difference is noted in the form of 'cracking' features in the sample that had been run in dry hydrogen. It is interesting to consider what the source of this microstructural change is, and whether it can be identified or correlated with EIS results.

Microstructural changes on the scale of crack formation can occur in an SOFC anode via various mechanisms. Stresses caused by thermomechanical factors can give rise to cracking of the electrodes or cells [21]. Volume expansion [21] and phase transformation of ceramic has been reported to be influenced by water under reduction process [22]; ceria can undergo reduction under very low pO_2 condition, leading to volume expansion and cracking. The exact cause of the electrode cracking phenomenon in this study is not clear and is the subject of ongoing study.

A large increase of the electrode LF arc in dry H_2 has been reported by Jiang and Badwal for Ni-YSZ cermet electrodes operating at 1273 K [14]. They propose that the mechanism and kinetics of the anode reaction is complex and strongly dependent on the catalytic activities of electrode materials (it being significantly different for Pt and Ni based systems), electronic conductivity of the electrolyte surface, and the water content in H_2 gas.

The transport of reactant species to three-phase-boundary (TPB) [23] includes gas diffusion through the porous material, dissociative adsorption of hydrogen (a very fast process at SOFC operating temperatures) and surface diffusion to the TPB sites, where reaction with oxide ion flux takes place [14,24]. The surface diffusion of H_2 species becomes faster as temperature increases [14]. The increase in the LF feature under dry operating conditions may therefore be attributed to slow surface diffusion of hydrogen, which is facilitated by the presence of oxide species in moist conditions. Fig. 5(b) shows

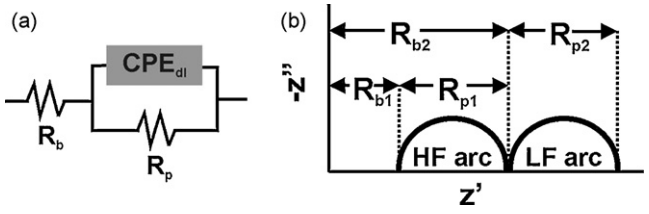

Fig. 8. (a) Equivalent circuit for used in extracting time constant following Eq. (2); and, (b) model explaining the use of Eq. (2) with the EIS response having two impedance arcs.

an increase of the LF feature with decreasing temperature, which supports this mechanism.

However, it should be noted that for the LF feature in dry fuel, a complete arc cannot be realised due to the low frequency limitation of the FRA. The polarization resistance fitting of the LF feature in the EIS response was assumed to be to a complete LF arc using a CPE element. The partial LF arc is sufficiently well defined, such that the fitting software reports an error of less than 4.6%. However, the fit cannot be unequivocally attributed to a single arc that intercepts the low frequency intercept, and does not contain any extra features.

When deriving a polarisation resistance from EIS measurements it is important to realise that processes other than those that represent losses in the electrochemical performance of an electrode may be detected. These may be manifestations of processes such as: species adsorption, microstructural change, corrosion, *etc*., which do not directly influence the performance of the fuel cell. Indeed, features may exist in EIS Nyquist plane representations which span a significantly larger part of the real axis range, than the point at which convergence with the real axis at the low frequency, (direct current (DC)), limit occurs.

In order to give more information on the processes occurring in moist and dry fuel, the time constant (τ) of impedance features in different fuel atmospheres were estimated and compared. The time constant (τ) is derived from:

$$\tau = R_p C \tag{1}$$

where R_p is the polarization resistance of the equivalent circuit, and C is the capacitance of the process. Extracting the time constant from an equivalent circuit containing a constant phase element is rather complicated, since it contains a distribution function [25]. For a system modelled with a CPE component, an approximate value of C can be derived using the approach of Brug et al. [19], as shown in Eq. (2):

$$C = \sqrt[n]{\frac{Q}{(1/R_b + 1/R_p)^{(1-n)}}} \tag{2}$$

where Q is a CPE and n is a CPE parameter. The R_b parameter in Eq. (2) represents the bulk resistance of the EIS response, while the R_p parameter represents the polarization resistance of that particular feature. If the impedance spectra exhibits two impedance features, as shown in Fig. 8(b) (high frequency impedance (HF); and low frequency impedance (LF)), then the value of R_b is derived from the value of high frequency intercept with the real axis (R_{b1}), while the value of R_b for the LF feature is obtained from the summation of the high frequency intercept and the HF arc width (R_{b1}). The value of R_p for the HF feature is the HF arc width (R_{p1}), while that for the LF feature is the LF arc width (R_{p2}). The approximated time constants for the HF and LF components of the cell exposed to dry and moist H_2 atmosphere for 60 h (Figs. 3 and 6) are shown in Table 1. It can be seen that the time constant of the HF impedance in dry atmosphere slightly increases compared to that in moist atmosphere, while the time constant of the LF component in dry conditions is considerably larger than that in moist conditions.

Table 1
The average time constant for HF, LF components of the impedance response of the half cell exposed to moist atmosphere (Fig. 3: 97% H_2, 3% H_2O, 873K) and dry atmosphere (Fig. 6: 97% H_2, 3% N_2, 873 K).

Time constant (τ)	Dry atmosphere (97% H_2, 3% N_2, 873 K)	Moist atmosphere (97% H_2, 3% H_2O, 873 K)
High frequency feature	0.12	0.08
Low frequency feature	44.93	0.58

It can be seen that the time constant of the process associated with the LF impedance feature when operated in dry H_2 is greater than 100 times that of the LF feature in moist hydrogen. It is difficult to unequivocally associate this to a particular mechanism; however, we can say that this is a very slow process and would not normally be expected to be associated with hydrogen surface diffusion at 873 K. However, we have shown that microstructural changes are discernable over a period of 24 h which may be the source of the large LF impedance feature in dry H_2.

4. Conclusions

The HF impedance in moist atmosphere varied largely with temperature while the LF impedance changed considerably with the H_2 content in the fuel. Therefore, in moist atmospheres, the HF component was attributed to charge transfer, while the LF component was associated with mass transport. In dry hydrogen, the HF impedance of the cell exposed to dry atmospheres increased slightly, but exhibited similar behaviour to that in moist atmospheres, namely increasing with decreased temperature. However the LF component of the symmetrical cell in dry atmosphere increased significantly, and exhibited a significantly slower time constant than that of the moist LF feature (ca. 100 times slower). This leads us to conclude that the low frequency feature exhibited by the dry system is not purely due to a mass transport imitation, but that a separate process is occurring that is thermally activated, since an increase in temperature results in a decrease in resistance. The thermal activation of the LF process supports the proposed mechanism of Jiang and Badwal which reported that the dissociative adsorption of hydrogen (H_{ad}) occurs favorably on a transition metal surface and the coverage of H_{ad} decreases with increased temperature, but as temperature increases, surface diffusion of H^+ species to the reactive sites becomes faster [14]. However, the origin of this LF feature may alternatively be associated with a slow corrosion-like process that results in microstructural damage of the anode, as shown by the cracking features in the SEM analysis. Further analysis at lower frequencies is required, but preliminary results show that EIS may be used as a diagnostic of microstructural change caused by operation at very low pO_2 conditions.

References

[1] N.Q. Minh, T. Takahashi, Science and Technology of Ceramic Fuel Cells, Elsevier Science, New York, 1995.
[2] S.P. Jiang, Y. Ramprakash, Solid State Ionics 122 (1999) 211.
[3] T.H. Etsell, S.N. Flengas, Electrochemical Science 118 (1971) 1980.
[4] A. Bieberle, L.J. Gauckler, Solid State Ionics 146 (2002) 23.
[5] M. Nagata, H. Iwahara, Journal of Applied Electrochemistry 23 (1993) 275.
[6] W.G. Bessler, 8th European SOFC Forum, Lucerne, Switzerland, 2008, p. B1101.
[7] M. Mogensen, in: S.C. Singhal, H. Iwahara (Eds.), Proceedings of the 3rd International Symposium on Solid Oxide Fuel Cells, 1993, p. 484.
[8] H. Zhu, R.J. Kee, W.M. Janardhanan, O. Deutscmann, D.G. Goodwin, Journal of the Electrochemical Society 152 (2005) A2427.
[9] S. Primdahl, M. Mogensen, Journal of the Electrochemical Society 144 (1997) 3409.
[10] P. Holtappels, I.C. Vinke, L.G.J. de Haart, U. Stimming, Journal of the Electrochemical Society 146 (1999) 2976.
[11] K.V. Hansen, K. Norrman, M. Mogensen, Journal of the Electrochemical Society 151 (2004) A1436.
[12] E.J.L. Schouler, M. Kleitz, Journal of the Electrochemical Society 134 (1987) 1045.

[13] N. Sakai, K. Yamaji, T. Horita, Y.P. Xiong, H. Kishimoto, M.E. Brito, H. Yokokawa, Solid State Ionics 174 (2004) 103.
[14] S.P. Jiang, S.P.S. Badwal, Journal of the Electrochemical Society 144 (1997) 3777.
[15] B.H.C. Steele, Solid State Ionics 129 (2000) 95.
[16] D.J.L. Brett, A. Atkinson, N.P. Brandon, S.J. Skinner, Chemical Society Reviews 37 (2008) 1568.
[17] S.A. Baron, N.P. Brandon, A. Atkinson, B.H.C. Steele, R. Rudkin, Journal of Power Sources 126 (2004) 58.
[18] B.A. Boukamp, Solid State Ionics 20 (1986) 31.
[19] G.J. Brug, A.L.G. van den Eeden, M. Sluyters-Rehbach, J.H. Sluyters, Journal of Electroanalytical Chemistry 176 (1984) 275.
[20] J.B. Jorcin, M.E. Orazem, N. Pébère, B. Tribollet, Electrochimica Acta 51 (2006) 1473.
[21] H. Yokokawa, H. Tu, B. Iwanschitz, A. Mai, Journal of Power Sources 182 (2008) 400.
[22] H. Kishimoto, N. Sakai, T. Horita, K. Yamaji, Y. Xiong, M.E. Brito, H. Yokokawa, Solid State Ionics 179 (2008) 2037.
[23] N.P. Brandon, D.J.L. Brett, Philosophical Transactions of the Royal Society 364 (2006) 147.
[24] S.C. Singhal, K. Kendall, High Temperature Solid Oxide Fuel Cells, Fundamental, Design and Application, Elsevier, Cornwall, 2003.
[25] I.D. Raistrick, D.R. Franceschetti, J.R. Macdonald, Impedance Spectroscopy Theory, Experiment and Applications, John Wiley & Sons, New Jersey, 2005.